Improved Receiver Architecture for Efficient Space-Based Massive ADS-B Signal Detection

Carlos Mosquera[1,*], Roberto López-Valcarce[1], Felipe Gómez-Cuba[1], Xavier Artiga[2], Pol Henarejos[2], and Nader Alagha[3]

[1] *atlanTTic Research Center, Universidade de Vigo, Spain*
[2] *Centre Tecnològic de Telecomunicacions de Catalunya (CTTC-CERCA), Castelldefels, Spain*
[3] *European Space Agency (ESA), Noordwijk, The Netherlands*
[*] *mosquera@gts.uvigo.es*

Keywords: ADS-B, LEO satellite, beamforming, signal detection, interference.

Abstract

Efficient detection of Automatic Dependent Surveillance–Broadcast (ADS-B) signals from low Earth orbit (LEO) satellites in highly congested airspaces remains a significant challenge, with room for potential improvement in the on-board multibeam antenna and digital baseband reception. A key limitation arises from message collisions at the 1090 MHz frequency, where overlapping ADS-B transmissions reduce detection performance. This work explores strategies to mitigate these effects, including a judicious beam selection to limit interference among signals, along with the application of advanced signal processing algorithms for enhanced detection and decoding.

1. Introduction

The increasing demand for global air traffic surveillance is driving innovation in technologies that extend beyond traditional ground-based systems. Automatic Dependent Surveillance-Broadcast (ADS-B) has emerged as a central technology for enabling precise, real-time aircraft tracking across both densely and sparsely populated airspaces. Originally developed for terrestrial use, ADS-B allows aircraft to automatically broadcast their position, velocity, identification, and other status information to any receiving station within line-of-sight. These messages, which are uncoordinated and broadcast periodically, have become a critical data source for air navigation service providers, researchers, and commercial tracking services [1].

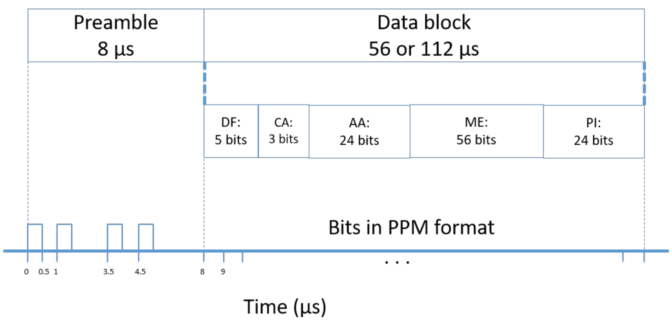

Fig. 1 Mode S message format.

ADS-B messages are sent from Mode S transponders, which encode data in Pulse Position Modulation (PPM) messages, following a preamble of 8 μs (Fig. 1). As opposed to many other Mode S types, ADS-B operates on a non-interrogation basis, with aircraft transmitting quasi-periodic messages, known as telegrams or *squitter* messages, in the 1090 MHz frequency band. This purely broadcast-based operation of ADS-B is carried out without coordination or scheduling among aircraft. As a result, multiple aircraft can transmit simultaneously, causing received signals to overlap, especially in regions with high traffic density. These overlapping messages lead to collisions, which pose a major challenge for any receiver attempting to detect and decode individual squitters.

The limitations of ground-based surveillance infrastructure, especially in remote, oceanic, or polar regions, have motivated the transition to space-based ADS-B. Satellites equipped with ADS-B receivers can provide truly global coverage, enabling real-time aircraft tracking even in areas beyond the reach of terrestrial radar and communication systems. Pioneering missions, such as ESA's Proba-V [2], have demonstrated the technical feasibility of receiving ADS-B messages from space. More recently, commercial services such as Aireon, hosted on the Iridium-NEXT constellation, have provided operational global ADS-B surveillance from orbit [3, 4]. The large Field of View (FoV) of satellites results in the simultaneous visibility of thousands of aircraft , each transmitting multiple uncoordinated ADS-B messages. The performance of a satellite ADS-B receiver is commonly evaluated using the Probability of Detection (PoD) metric, defined as the ratio of successfully decoded messages to the number of expected transmissions. Measurements from Proba-V [1] have shown that PoD can drop significantly in dense airspace or coastal handoff zones. Note that a large concentration of interfering aircraft is expected from the vicinity of major airports, and also from the peripheral view (horizon) of the satellite, with lots of aircraft per angular section.

This paper explores advanced receiver architectures for emerging space-based ADS-B systems able to manage high levels of interference, which are becoming more prevalent as the world air traffic keeps growing. The study addresses the ADS-B subsystem on-board the satellite, in particular the antenna array and the baseband receiver. Processing takes place at beam level, with the design effort oriented towards the beamforming strategies and the advanced detection algorithms able to cope with low Signal to Noise Ratio (SNR) and overlapping messages.

2. System Specifications

We consider a single LEO satellite with a planar square array of 8×8 elements with half-wavelength separation, corresponding to an approximate area of one square meter. The elements are assumed to be microstrip patches modeled with a gain of 5.5 dBi, and a radiation pattern following a $\cos^2(\theta)$, being θ the angle from nadir. Multiple beams are generated by appropriately weighting the array signals, enabling spatial selectivity and reducing interference through sectorization of the field of view. The type and number of beams will be the subject of study in Section 3.

To successfully *detect and decode* an ADS-B message received in a given beam, a receiver must perform three critical tasks:

1) **Preamble detection.** Identify the start of the message using its distinct 8-microsecond preamble, which consists of four fixed PPM-encoded pulses at precise time intervals. The message detection may also benefit from the knowledge of additional symbols within specific ADS-B messages.
2) **Message demodulation.** Accurately sample and decode the 112-bit message using PPM decoding logic. This requires adequate signal strength and timing synchronization.
3) **CRC verification.** Validate the integrity of the message using the embedded 24-bit cyclic redundancy check (CRC). Only messages that pass CRC verification are considered valid and usable.

These steps must be completed within a tight time window and under potentially poor signal conditions, especially for receivers operating from space, where signal attenuation, Doppler shift, and overlapping transmissions are prevalent. In addition to the ADS-B telegrams from other aircraft , replies contribute to the interference encountered by ADS-B receivers. Replies are sent in response to: (i) ground- to-air interrogations sent by secondary surveillance radars (SSR); and (ii) air-to-air interrogations sent by ACAS (Airborne Collision Avoidance System), also known as TCAS (Traffic Collision Avoidance System). The frequency band of all these replies is also 1090 MHz. While legacy systems operate with Mode A/C replies, Mode S is progressively taking over [5].

The probability of meeting an update interval, *i.e.*, the probability of successfully detecting a position message within a given interval T, is known as the *Probability of Update Interval (T seconds) -* $PUI(T)$. The performance of Air Traffic Systems (ATS) surveillance is strictly defined and regulated through organizations such as EUROCAE [6]. This value is required to be $PUI(T) \geq 95\%$, with the update interval T in the range 5 to 8 seconds, depending on the specific case. For example, Aireon reported in 2021 a goal of $PUI(8) \geq 96\%$*. Due to the high amount of exchanged messages at 1090 MHz, $PUI(T)$ requirements can be hard to meet at certain locations, due to the large footprint of beams, especially at the edge of the coverage area.

Potential improvements lie in the design of novel preamble and data detection schemes aimed at enhancing performance under collision scenarios, particularly in regions with high aircraft density. Additionally, the design of the beam pattern may significantly influence the probability of detection. In this work we have explored these avenues of research, and obtained some relevant insights for the operation of ADS-B reception from space. In particular, coherent detection, interference-aware maximum *a posteriori* (MAP) decoding, and beam oversampling, emerge as instrumental enablers. Each of these techniques can improve the metrics of ADS-B reception, and their combined use holds promise for even greater gains. Further details are presented in the following sections.

*Space-Based ADS-B - Details and Uses. ICAO meeting, 2021.

2.1 Traffic Characterization

ADS-B messages are transmitted periodically with random jitter. For example, airborne position squitter transmissions are emitted at random intervals that are uniformly distributed over the range from 0.4 to 0.6 seconds, using a time quantization grid which may differ across different transponders. Note that this rate can change when the aircraft is on the ground [7]. As mentioned in the Introduction, ADS-B messages are sent from an aircraft at an average rate of 6.2 messages per second, alternating transmissions between top and bottom antennas†. This includes the two position messages per second, whose successful decoding statistics are the most critical performance indication of an ADS-B based surveillance system.

In addition to the extended squitter (1090 ES), the 1090 MHz frequency is also used for replies to the different interrogations sent from ground radars and other aircraft. These requests, sent in the uplink, are transmitted using the 1030 MHz radio frequency, and trigger the following replies:

- **Mode A/C replies**. Triggered by Secondary Surveillance Radar (SSR), short replies, legacy systems, gradually being phased out.
- **Mode S replies**. Triggered by Mode S ground radars and TCAS/ACAS airborne systems. There are two types which differ in their duration: Short Squitter (56 μs) and Long Squitter (120 μs).

For the purpose of characterizing packet traffic and testing detection algorithms, ADS-B broadcast messages and Mode S replies (triggered by SSR or TCAS) will be considered. SSR (Mode A/C) messages will not be included, as multiple sources concur on their declining use, particularly noting that they are not emitted from the top-mounted antennas [5]. Note that only messages sent from the top antenna of aircraft are assumed to be detectable from LEO satellites. For simplicity in the simulations, the rate of Mode S messages will be assumed to be constant over time, and the same for all aircraft, as per Table 1. In practice, these reply messages will be triggered by external interrogations, with a frequency and timing depending on factors such as the presence of ground radars and the proximity of other airplanes.

The evaluation is carried over an aircraft distribution captured on the first of June of 2025 with the satellite flying at an orbit of 550 km at 41° latitutde, 10° longitude (Central Europe). Unless otherwise stated, the main simulation parameters used are summarized in 1. We consider as potentially visible aircraft those located on a satellite footprint delimited by the region in which the satellite is seen at an elevation of 0°, although a minimum elevation angle will be required for practical operation.

†The use of two antennas, one on top of the fuselage and one on the bottom, reduces the impact of potential shadowing by the fuselage.

For the scenario under test, this corresponds to a maximum satellite tilt angle (with respect to nadir) of 67° and to 4550 visible aircraft.

For initial testing purposes, the parameters in Table 1 have been used.

Table 1 Basic testing parameters.

Parameter	Value/description
Transponder power distribution	125 W (25%) 250 W (50%) 500 W (25%)
Message rate (top antenna)	3 (ADS-B), 6 (Mode S replies) messages/s
Aircraft antenna	As per ITU report [5, p. 5]
Satellite Antenna	8×8 array, $\lambda/2$ separation (1 sqm)
Antenna element gain	5.5 dBi
Antenna element radiation pattern	$\cos^2 \theta$
Receiver bandwidth	2 MHz
Receiver noise temperature	500°K
Number of beams	Hundreds
Satellite orbit height	550 km
Frequency	1090 MHz
Additional losses (propagation and polarization)	3.7 dB
Air traffic snapshots	Source: ADS-B Exchange

3. Multibeam layout design

In this section we analyze the impact of the beam layout design on the probability of aircraft detection, so that beam layout guidelines can be extracted for practical designs. The metric for the evaluation is the probability of aircraft detection with an update interval of 8 seconds, $PUI(8)$, as defined in Section 2. Its evaluation involves: (i) the generation of the satellite beam layout; (ii) calculation of the received SNR per aircraft and per beam; (iii) generation of a traffic pattern over a window of 8 s; (iv) computation of Signal to Interference and Noise Ratio (SINR) and counting of detected messages per aircraft and per beam. As a simple initial rule to implement, a message is considered detected if the whole packet is collision-free and received with a minimum SNR_{th}=8 dB. More refined detection schemes will be detailed in Section 4. As expected, the probability of detection and, consequently, $PUI(8)$, depends on the aircraft density, air traffic patterns, message rate and the beam layout. ADS-B reception can only act on the latter, which is the object of this section.

For benchmarking purposes, we consider a uniform hexagonal grid of beams covering the satellite field of view, that as discussed before comprises a maximum angle from nadir of 67°. The beam layout is designed with an angular beam separation (ABS) between beam centers in the UV coordinates of

$$ABS = \sqrt{3} \sin \frac{HPBW}{2 \cdot BoF}, \tag{1}$$

where $HPBW$ is the half-power beamwidth of the satellite antenna and BoF a beam overlapping factor. BoF=1 corresponds to a beam crossover of -3 dB and a total number of 97 beams. Fig. 2 depicts the superposition of the corresponding beam layout and the aircraft distribution in the UV coordinates. Even though the aircraft distribution is rather uniform over Europe in geodetic coordinates, large aircraft densities take place at the edge of the satellite coverage due to the projection of the beam footprints on Earth. Such large densities translate into a degraded $PUI(8)$ in those regions, to be addressed below. It is also noteworthy that some aircraft go undetected in low density regions, for instance around (u=0,v=0.5). For a closer look, Fig. 3 shows the radiation pattern of a beam pointing to that region, overlapped on the set of detectable aircraft (with $SNR \geq SNR_{th}$) and those actually detected. The explanation behind the missing detections in this area is twofold. On the one side, the phased-array synthesis of the different beams, with constant amplitude weights, gives rise to significant sidelobes (up to -13 dB), which leak signals into the main beam[‡]. Additionally, a detailed analysis shows that aircraft in this region display a notch in the antenna radiation pattern towards the satellite, which can be observed in [5, p. 5]. The two above effects combine to degrade the $PUI(8)$ in the ring with a tilt angle from nadir of 30° approximately. A tentative solution for that is the use of amplitude tapering to control the sidelobe levels at the expense of larger HPBWs.

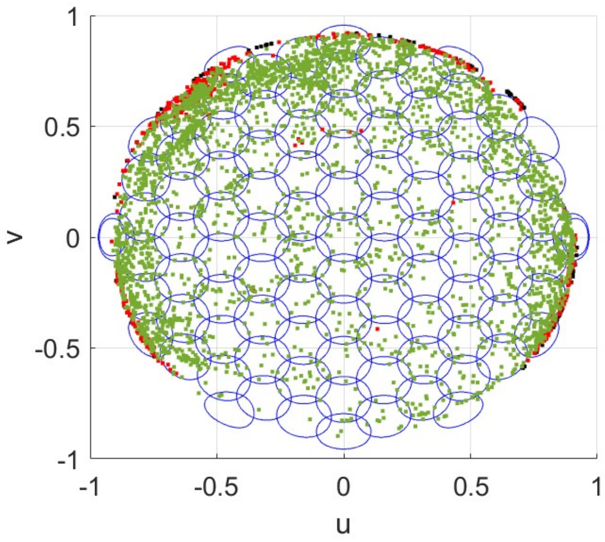

Fig. 2 Benchmark beam layout with BoF=1 and aircraft distribution: detected aircraft (green), not detected aircraft due to interference (red), non detected aircraft due to low SNR (black).

As mentioned above, coverage at the edge of the footprint is especially critical, due to the combination of limited SNR and high aircraft density, with the resulting degradation of $PUI(8)$. For illustration purposes, Fig. 4 zooms into one sector at the edge of Fig. 2. As a countermeasure, we advocate for larger beam overlapping, by increasing the number of beams through the appropriate beam oversampling. It is expected that the resulting diversity will increase the chances to detect the "critical" aircraft,

[‡]At the same time, some aircraft can be potentially detected from sidelobe beams.

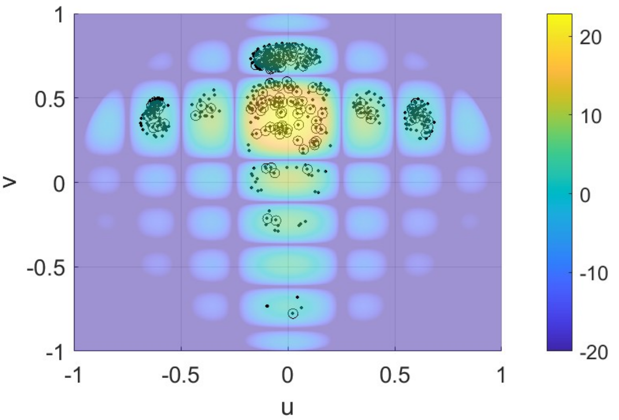

Fig. 3 Superposition of the radiation pattern of one beam, the aircraft displaying $SNR \geq SNR_{th}$ (dots), and the aircraft detected by that beam (circles) in one second.

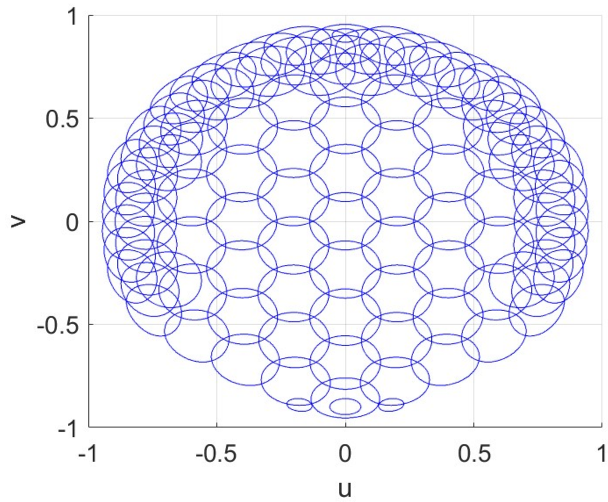

Fig. 5 Beam layout with BoF=2 for θ>50° and $|\phi|$ < 120°.

which may fall in more favorable locations on some of the extra beams. Fig. 5 depicts a case where the beam density in the region with high aircraft density has been increased to BoF = 2.

Let us now compare the performance of the benchmark layout (with BoF = 1) with the combination of amplitude tapering and beam overlapping. In particular, we consider three combinations: (i) Taylor amplitude tapering with sidelobe levels below -30 dB; (ii) Taylor amplitude tapering with sidelobe levels below -30 dB and BoF = 2 for θ>50° and $|\phi|$ < 120°; and (iii) Taylor amplitude tapering with sidelobe levels below -30 dB and BoF = 4 for θ>50° and $|\phi|$ < 120°. Let us remark that the beamwidth with the Taylor window raises from 12.6° to 16°. As shown in Table 2, the Taylor tapering solution, despite implying a reduction of 30% in the number of beams, provides a 5.7 percentage points improvement with respect to the benchmark. Moreover, the beam diversity solutions provide further improvements between 5-6 percentage points.

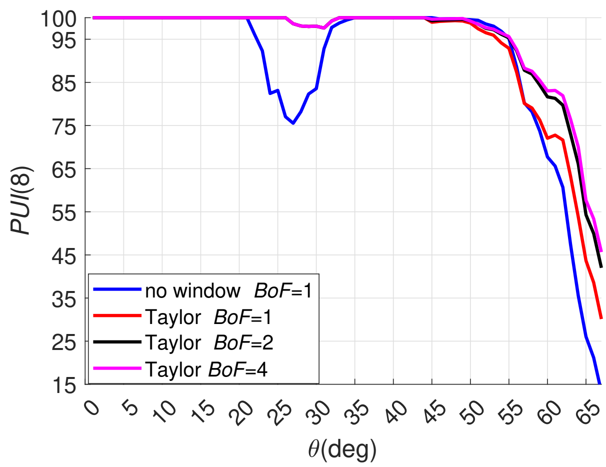

Fig. 6 $PUI(8)$ as a function of the tilt angle from the satellite.

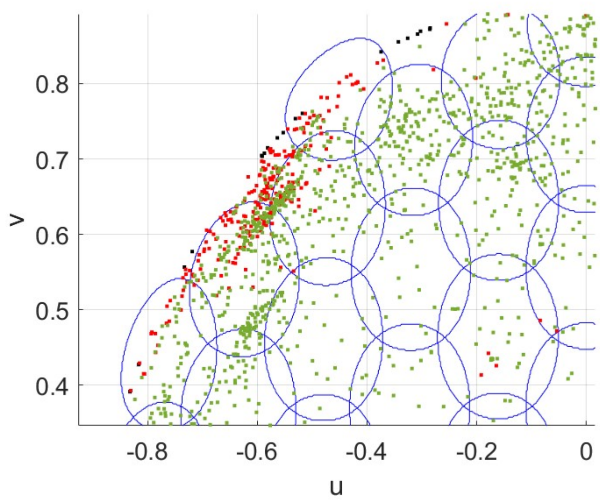

Fig. 4 Detail at the coverage edge of beam layout with BoF=1 and aircraft distribution: detected aircraft (green), not detected aircraft due to interference (red), non detected aircraft due to low SNR (black).

Finally, Fig. 6 evaluates how the $PUI(8)$ evolves with the tilt angle with respect to nadir for the four beamforming configurations. Its evaluation entails the use of a sliding window of 5° for averaging the number of detected and detectable aircraft for each θ. Fig. 6 illustrates the anticipated degradation of $PUI(8)$ between 25° and 30° for the baseline beam layout, in the absence of tapering, due to the interplay of high sidelobe levels and the dip in the aircraft radiation pattern. Clearly, Taylor tapering fixes this issue. Besides, beam overlapping at coverage edge improves the detection beyond 55°, even though the improvement is moderate with diminishing returns for higher BoF.

4. Physical Layer Receiver

The decoding of the received ADS-B messages entails a number of tasks which include preamble detection, synchronization, message demodulation and CRC verification. All this needs to be done in the presence of the potential interference caused by the collisions of simultaneous messages. In this section we describe the basic features of an advanced interference-aware coherent receiver, able to cope with the collision of at least

Table 2 Beamforming comparison.

Scheme	Number of beams	$PUI(8)$
Baseline (no window taper, $BoF = 1$)	97	73.9%
Taylor taper, $BoF = 1$	61	79.6%
Taylor taper, $BoF = 2$ at coverage edge	112	84.7%
Taylor taper, $BoF = 4$ at coverage edge	290	85.9%

a strong mode S interfering message, and which extends the range of operation of traditional envelope detectors. Note that, if applied in conjunction with the beamforming strategies of the previous section, this is expected to improve the metrics presented in the previous paragraphs.

4.1 Preamble Detection

If ADS-B transmitters can be assumed to maintain phase coherence during their transmissions, *i.e.,* messages are generated by modulating a carrier waveform rather than by on/off switching an oscillator, then coherent preamble detection becomes feasible, in contrast with previous incoherent approaches which only used the envelope of the received signal [8–10].

Preamble detection must be carried out sequentially in time, since the arrival time of the message is unknown. For a given window position, a vector of samples is obtained and one is to make a decision regarding the following hypotheses:

- H_0: The ADS-B preamble is not present in the observed vector, which contains noise and interference only;
- H_1: The ADS-B preamble is present in the observed vector.

Let the samples of the known preamble be denoted by $c(k)$, $k = 0, 1, \ldots, K-1$. Suppose that detection is performed based on the signal from a single beam (the "beam under test"), and let $x(k)$, $k = 0, 1, \ldots, K-1$, be the observed samples. The hypothesis test can be written as:

$$\begin{array}{llll} H_0: & x(k) & = & z(k) + \eta(k), \\ H_1: & x(k) & = & h_0 e^{\jmath 2\pi \nu_0 k} c(k) + z(k) + \eta(k), \end{array} \tag{2}$$

for $k = 0, 1, \ldots, K-1$, where h_0 and $\nu_0 \in [0, 1)$ are respectively the complex gain and normalized carrier frequency offset (CFO) affecting the preamble, $\{\eta(k)\}$ is circularly-symmetric AWGN with zero mean, and $z(k)$ captures the interference due to other aircraft:

$$z(k) = \sum_{i=1}^{I} h_i e^{\jmath 2\pi \nu_i k} s_i(k - d_i). \tag{3}$$

In (3), I is the number of interferers present, whereas h_i, ν_i and d_i respectively denote the complex gain, CFO and delay affecting the signal $s_i(k)$ emanating from the i-th interferer.

We approach this detection problem from a Generalized Likelihood Ratio Test (GLRT) perspective, since there are unknown nuisance parameters under both hypotheses. In fact, even the *number* of such parameters associated to the interference term $z(k)$ is unknown (since I is unknown). Thus, to make the problem tractable, we make the assumption that $z(k) + \eta(k)$ can be approximated as Gaussian, with zero mean and unknown variance σ^2. Thus, the unknown parameters are $\boldsymbol{\theta}_0 = \{\sigma^2\}$ under H_0, and $\boldsymbol{\theta}_1 = \{h_0, \nu_0, \sigma^2\}$ under H_1. The GLRT is formulated as

$$\frac{p_1(\boldsymbol{x}; \hat{\boldsymbol{\theta}}_1)}{p_0(\boldsymbol{x}; \hat{\boldsymbol{\theta}}_0)} \underset{H_0}{\overset{H_1}{\gtrless}} \gamma' \tag{4}$$

where γ' is a suitable threshold, $p_i(\boldsymbol{x})$ is the probability density function (pdf) of the observed vector $\boldsymbol{x}$ under H_i, $i \in \{0, 1\}$, and $\hat{\boldsymbol{\theta}}_i$ is the maximum likelihood (ML) estimate of $\boldsymbol{\theta}_i$ under H_i. Note, under the Gaussian assumption,

$$p_i(\boldsymbol{x}; \boldsymbol{\theta}_i) = \frac{1}{(\pi\sigma^2)^K} \exp\left\{-\frac{1}{\sigma^2} \sum_{k=0}^{K-1} |x(k) - a_i(k)|^2\right\}, \tag{5}$$

with $a_0(k) = 0$ and $a_1(k) = h_0 e^{\jmath 2\pi \nu_0 k} c(k)$. The required ML estimates can be obtained in closed form, except for the CFO. The final form of the GLRT is readily seen to be statistically equivalent to

$$\max_{0 \le \nu < 1} |\hat{\rho}(\nu)|^2 \underset{H_0}{\overset{H_1}{\gtrless}} \gamma \tag{6}$$

with γ a threshold, and with $\hat{\rho}(\nu)$ the normalized cross-correlation coefficient between the observed signal and the CFO-corrected preamble:

$$\hat{\rho}(\nu) = \frac{\sum_{k=0}^{K-1} c^*(k) x(k) e^{-\jmath 2\pi \nu k}}{\sqrt{\sum_{k=0}^{K-1} |x(k)|^2 \cdot \sum_{\ell=0}^{K-1} |c(\ell)|^2}}. \tag{7}$$

A numerically efficient means to implement (6) via FFT is to discretize the range of normalized CFO values as $\nu = \frac{n}{N}$, $n = 0, 1, \ldots, N-1$ with $N \ge K$, and then note that

$$\sum_{k=0}^{K-1} c^*(k) x(k) e^{-\jmath \frac{2\pi}{N} nk} \tag{8}$$

is the N-point DFT of the (zero-padded) sequence $c^*(k)x(k)$.

To illustrate the performance of the GLRT detectors, we consider both medium-density and high-density areas. As in [10], the extended preamble to be detected is 13 μs long, and consists of the ADS-B preamble together with the DF field (DF = 17), see Fig. 1. The sampling rate equals $M = 4$ times the chip rate, so that the extended preamble is 104 samples long. The SNR is set as the average energy of the extended preamble observed at any array element over the AWGN variance at that element, thus a pre-beamforming SNR. The noise variance is uniform across array elements, and the observation window equals the length of the extended preamble.

Fig. 7 shows the receiver operating characteristics (ROC) curves for two single-beam detectors: the coherent GLRT detector (6) and the incoherent GLRT detector proposed in [10]. It is clear that, if coherent operation is feasible, the corresponding detector provides a significant advantage over the noncoherent scheme, basically at the cost of an additional FFT operation. The degradation in detection performance due to the increased interference in high-density areas is clearly seen.

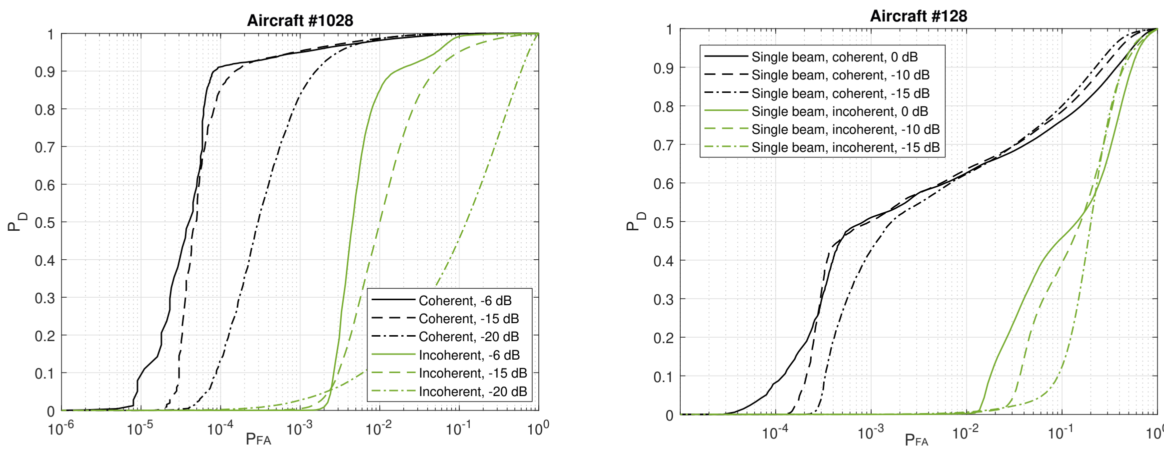

(a) Medium-density area (27 aircraft in the beam).

(b) High-density area (113 aircraft in the beam).

Fig. 7 ROC curves for single-beam detectors under different SNR. Note: the reported SNR values are normalized representations of higher actual SNR levels. Number of beams: 91, hexagonal grid.

4.2 Data Demodulation

The ADS-B ICAO standard [11] establishes that receivers of category 1, 2 and 3 must be equal or better than the "multi-sample technique" implementation reference in the appendix of the DO-260B Minimum Operational Performance Standard (MOPS) document [12]. One particular property of this technique is that it removes interference during symbol detection by exploiting knowledge of the signal amplitude (estimated preamble level). The rationale behind this receiver follows the insights provided in the so-called multi-sample technique in [13]: for a known preamble level, if one half PPM pulse has the same level as the preamble level, and a pulse much greater than the preamble level is in the other half, we can in fact recognize that the latter of the two is interference. The multi-sample technique in [13] counts how many samples in/out of preamble level are present in each half-pulse. Along this vein, we have derived an optimal Maximum *A Posteriori* (MAP) symbol detector in the presence of interference that explains why this technique works well under Mode A/C collisions. The analytical MAP decoder for Mode S collisions has also been derived. In both cases coherent detection has been enforced, with random phase and CFO across the different signals. The DO-260B multi-sample and enhanced receiver techniques are a particular instance of our MAP receiver, by assuming no phase or CFO, and a (possibly) Mode AC collision for each single bit.

The MAP decoder finds the maximum of the averaged *a posteriori* probability function of the channel output in Eq. 2:

$$\hat{b} = \max_b \mathscr{L}_{\boldsymbol{x}}(b) = \max_b \int f(\boldsymbol{x}|b,z)f(z)dz. \tag{9}$$

Efficient receivers to maximize this function are often implemented using the Log Likelihood Ratio (LLR), which translates the problem into a GLRT similar to the preamble detection problem:

$$\log \frac{\mathscr{L}_{\boldsymbol{x}}(1)}{\mathscr{L}_{\boldsymbol{x}}(0)} \underset{H_0}{\overset{H_1}{\gtrless}} 0. \tag{10}$$

The model of the interference $z(k)$ in (2) is instrumental for the operation of MAP decoding. We assume that there is a known probability of interference during each bit, given by P_I, so the distribution of z reads as

$$(1 - P_I)\delta(0) + P_I f(z|I). \tag{11}$$

The probability P_I depends on the expected rate of messages, which is a function of the air traffic and geographical location. On the other hand, coming up with a statistical model for $f(z|I)$ is more challenging, since it entails the relative time shift and amplitude, and phase/frequency offset of the interfering pulse with respect to the intended signal. The mathematical details will be skipped here for the sake of the presentation.

In order to illustrate the potential of our MAP decoder, we operate with the incoming stream of a given beam, with no CFO and no phase in the interference, which is assumed to be a Mode S collision. This type of collisions are widely considered as unresolvable and leading to 100% packet loss in the literature of DO-260B [3]. This is because these collisions are not featured in the Look Up Table (LUT) "empirical pdf" derived in [13][§]. Note that mode A/C messages have a duration of $20.3\mu s$, much shorter than the $120\mu s$ duration of (long format) mode S messages.

In Fig. 8 we depict the BER for 10^5 Monte Carlo single-bit simulations for a multi-sample receiver with $M = 4$ samples per chip (8 samples per PPM symbol). The Treat Interference as Noise (TIN) receiver finds the nearest symbol to the observed samples, which is optimal in the Additive White Gaussian Noise (AWGN) case, in the absence of interference. Both DO-260B receiver and MAP receiver, designed to operate like the DO-260B standard, suffer a catastrophic degradation of the performance. This is because both receivers are designed specifically to reverse the effects of Mode AC collisions, and produce a significant number of errors under Mode S collisions.

[§]The LUT techniques proposed in [13], also discussed in the enhanced receivers of the standard [12], are based on the same MAP principle that we are adopting. However, instead of an analytically tractable *a priori* distribution, the LUT techniques employ an empirical aproximation of the pdf obtained by massive Monte Carlo simulation:

$$\hat{f}^{\mathrm{LUT}}(b|\boldsymbol{x}) = \frac{\texttt{\# times received } \boldsymbol{x} \texttt{ with tx. bit } b}{\texttt{\# times received } \boldsymbol{x}}$$

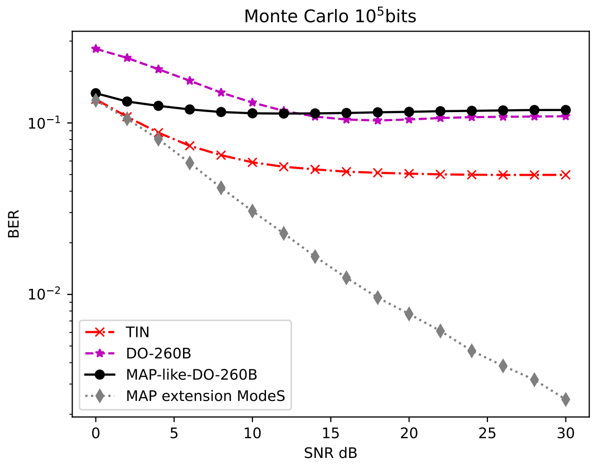

Fig. 8 BER in the presence of a Mode S collision, $M = 4$, no CFO.

Finally, our MAP receiver with a correct assumption of a Mode S *a priori* distribution of the interference (gray) is able to mitigate the impact of the collision and deliver one order of magnitude improved BER without a performance floor in the high SNR regime. The practical impact under real traffic patterns, as well as the critical importance of calibrating the interference-aware MAP detector, remains to be analyzed.

Although not shown here, the improvement is more noticeable with complex IQ coherent receivers, where the random phase and CFO difference between the desired signal and the interferers improves the ability to mitigate the collisions.

5. Conclusions

The pressing need for improved ADS-B detection schemes from space, able to cope with the growing levels of air traffic, has motivated this work on advaced receiver architectures for emerging ADS-B payloads. Beam oversampling, coherent detection and MAP decoding have been identified as key drivers to improve the probability of detection, in particular in those beams with higher traffic density. The size constraints of the satellite antenna array limits the resolution of the beams, with wide footprints potentially encompassing more than a hundred aircraft, giving rise to message collisions. We have seen how the reduction of sidelobe levels, despite increasing the beamwidth, and beam diversity through increasing beam density, are both beneficial for improving the probability of detection. However, increasing the number of beams raises receiver complexity so an efficient map between aircraft density and map density is still an open area of research. Moreover, the effectiveness of increasing beam density is limited at extreme coverage angles, so new beam diversity solutions addressing these regions need to be investigated. Initial results on multibeam/MIMO detection not shown here have also been obtained, displaying additional performance gain in terms of preamble detection and data demodulation.

Acknowledgment

This work has been supported by the European Space Agency (ESA) funded activity SATELLITE NETWORK OF EXPERTS V (4000130962/20/NL/NL/FE), under the Work Item 4.5: Receiver Front-end Architecture for Efficient Massive ADS-B Signal Detection. The views of the authors of this paper do not necessarily reflect the views of ESA. Also funded in part by MCIN/AEI/10.13039/501100011033/ FEDER "A way of making Europe" under project MAYTE (PID2022-136512OB-C22), and by Spanish Ministerio de Ciencia e Innovación (MICINN), project CASTRO (PID2021-122483OA-I00).

References

[1] J. Budroweit, F. Eichstaedt, and T. Delovski, "Aircraft surveillance from space: The future of air traffic control?: Space-based ADS-B, status, challenges and opportunities," *IEEE Microwave Magazine*, vol. 25, no. 12, pp. 68–76, 2024.

[2] K. Werner, J. Bredemeyer, and T. Delovski, "ADS-B over satellite: Global air traffic surveillance from space," in *2014 Tyrrhenian International Workshop on Digital Communications - Enhanced Surveillance of Aircraft and Vehicles (TIWDC/ESAV)*, (Rome, Italy), pp. 47–52, IEEE, Sept. 2014.

[3] M. A. Garcia, J. Stafford, J. Minnix, and J. Dolan, "Aireon space based ADS-B performance model," in *2015 Integrated Communication, Navigation and Surveillance Conference (ICNS)*, pp. C2–1–C2–10, Apr. 2015. ISSN: 2155-4951.

[4] M. A. Garcia, J. Dolan, and A. Hoag, "Aireon's initial on-orbit performance analysis of space-based ADS-B," in *2017 Integrated Communications, Navigation and Surveillance Conference (ICNS)*, pp. 4A1–1–4A1–8, Apr. 2017.

[5] "Reception of automatic dependent surveillance broadcast via satellite and compatibility studies with incumbent systems in the frequency band 1,087.7-1,092.3 MHz," *Report ITU-R M.2413-0*, 2017.

[6] EUROCAE, "Technical Specification for a 1090 MHz Extended Squitter ADS-B Surveillance System," *ED-129C*, 2022.

[7] International Civil Aviation Organization, "Annex 10 to the Convention on International Civil Aviation: Aeronautical Telecommunications, Volume IV – Surveillance and Collision Avoidance Systems," tech. rep., ICAO, Montreal, Canada, 2014. Available from https://www.icao.int.

[8] H. Zou, T. Ban, and Z. Zhuang, "An S Mode ADS-B preamble detection algorithm," in *2019 IEEE 5th International Conference on Computer and Communications (ICCC)*, pp. 178–182, 2019.

[9] P. Ren, J. Wang, H. Song, P. Zhang, and T. Ban, "A novel multi-criteria preamble detection algorithm for ADS-B signals," *IEEE Access*, vol. 7, pp. 97319–97332, 2019.

[10] M. Morelli, M. Moretti, and N. Alagha, "GLRT preamble detection for satellite ADS-B," in *40th International Communications Satellite Systems Conference (ICSSC 2023)*, vol. 2023, pp. 195–201, 2023.

[11] *Aeronautical Telecommunications: International Standards and Recommended Practices. Volume IV, Surveillance Radar and Collision Avoidance Systems*. Montreal, Quebec, Canada: International Civil Aviation Organization, fifth edition ed., 2014.

[12] Radio Technical Commission for Aeronautics (RTCA), "Minimum Operational Performance Standards for 1090 MHz Extended Squitter Automatic Dependent Surveillance–Broadcast (ADS-B) and Traffic Information Services–Broadcast (TIS-B)," *RTCA DO-260B*, 2009.

[13] W. Harman, J. Gertz, and A. Kaminsky, "Techniques for improved reception of 1090 MHz ADS-B signals," in *17th DASC. AIAA/IEEE/SAE. Digital Avionics Systems Conference. Proceedings (Cat. No.98CH36267)*, vol. 2, (Bellevue, WA, USA), pp. G25/1–G25/9, IEEE, 1998.